JACS
JOURNAL OF THE AMERICAN CHEMICAL SOCIETY
Article
pubs.acs.org/JACS

Dissecting Multivalent Lectin–Carbohydrate Recognition Using Polyvalent Multifunctional Glycan-Quantum Dots

Yuan Guo,*[,†] Inga Nehlmeier,[§] Emma Poole,[†] Chadamas Sakonsinsiri,[†,#] Nicole Hondow,[‡] Andy Brown,[‡] Qing Li,[∥] Shuang Li,[⊥] Jessie Whitworth,[†] Zhongjun Li,[∥] Anchi Yu,[⊥] Rik Brydson,[‡] W. Bruce Turnbull,[†] Stefan Pöhlmann,[§] and Dejian Zhou*[,†]

[†]School of Chemistry and Astbury Centre for Structural Molecular Biology, and [‡]School of Chemical and Process Engineering, University of Leeds, Leeds LS2 9JT, United Kingdom

[§]Infection Biology Unit, German Primate Center, Kellnerweg 4, Gottingen 37077, Germany

[∥]Department of Chemical Biology, Peking University Health Sciences Centre, Beijing 100191, People's Republic of China

[⊥]Department of Chemistry, Renmin University of China, Beijing 100872, People's Republic of China

Supporting Information

ABSTRACT: Multivalent protein–carbohydrate interactions initiate the first contacts between virus/bacteria and target cells, which ultimately lead to infection. Understanding the structures and binding modes involved is vital to the design of specific, potent multivalent inhibitors. However, the lack of structural information on such flexible, complex, and multimeric cell surface membrane proteins has often hampered such endeavors. Herein, we report that quantum dots (QDs) displayed with a dense array of mono-/disaccharides are powerful probes for multivalent protein–glycan interactions. Using a pair of closely related tetrameric lectins, DC-SIGN and DC-SIGNR, which bind to the HIV and Ebola virus glycoproteins (EBOV-GP) to augment viral entry and infect target cells, we show that such QDs efficiently dissect the different DC-SIGN/R-glycan binding modes (tetra-/di-/monovalent) through a combination of multimodal readouts: Förster resonance energy transfer (FRET), hydrodynamic size measurement, and transmission electron microscopy imaging. We also report a new QD-FRET method for quantifying QD-DC-SIGN/R binding affinity, revealing that DC-SIGN binds to the QD >100-fold tighter than does DC-SIGNR. This result is consistent with DC-SIGN's higher trans-infection efficiency of some HIV strains over DC-SIGNR. Finally, we show that the QDs potently inhibit DC-SIGN-mediated enhancement of EBOV-GP-driven transduction of target cells with IC_{50} values down to 0.7 nM, matching well to their DC-SIGN binding constant (apparent K_d = 0.6 nM) measured by FRET. These results suggest that the glycan-QDs are powerful multifunctional probes for dissecting multivalent protein–ligand recognition and predicting glyconanoparticle inhibition of virus infection at the cellular level.

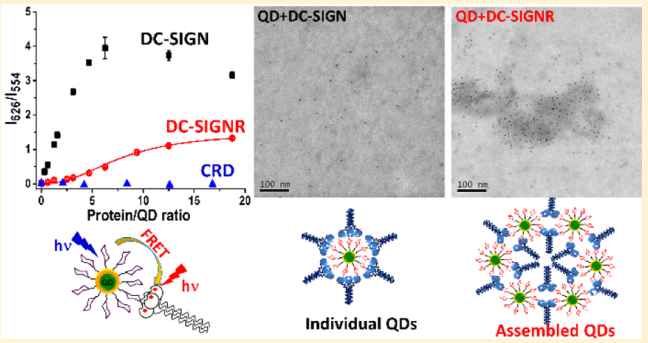

INTRODUCTION

Multivalent protein–carbohydrate interactions are widespread in biology and play a central role in many important biological events, including viral and bacterial infection, cell–cell communication, and host immune response regulation.[1−5] Such interactions initiate the first contact between pathogens (e.g., viruses and bacteria) and target cells that ultimately leads to infection. However, monovalent protein–glycan interactions are intrinsically weak, and hence biologically inactive. To compensate this limitation, pathogens display arrays of specific glycans on their surface, allowing them to bind efficiently to multimeric glycan-binding proteins (lectins) on target cell surfaces and to exploit multivalency to enhance binding affinity and gain cell entry, which ultimately leads to infection.[3−6] Therefore, these multivalent interactions are attractive targets for developing novel antiviral interventions, especially entry inhibitors, which can minimize virus resistance development.[1−5,7] In this regard, the spatial- and orientation-match between the viral surface glycans and carbohydrate recognition domains (CRDs) of cell surface lectins is key to enhance binding affinity and specificity.[8,9] Therefore, understanding the structure and spatial arrangement of the multivalent binding partners is essential for antiviral intervention, which has been the focus of significant current research.[1−5,7,10]

Synthetic glycoconjugates can block pathogen–lectin interactions whose inhibitory potency critically depends on the spatial- and orientation-match between the multivalent binding partners.[3,8−14] However, a major challenge is the lack of structural information for many cell surface multimeric lectins,

Received: May 17, 2017
Published: August 8, 2017

DOI: 10.1021/jacs.7b05104
J. Am. Chem. Soc. 2017, 139, 11833−11844

due to the problems associated with solving the structure of such flexible, complex, and multimeric membrane proteins by X-ray crystallography. For example, despite extensive research over the past two decades, the complete crystal structures of two important pathogen receptors, the tetrameric dendritic cell receptor, DC-SIGN,[15−20] and its closely related endothelial cell receptor DC-SIGNR[21] (collectively abbreviated as DC-SIGN/R hereafter), remain unknown apart from a structure model built upon the solution X-ray scattering data.[20] These two receptors play a key role in promoting HIV/Ebola virus (EBOV) infection by binding to multiple mannose-containing glycans on the virus surface.[15,18,19,21−23] Interestingly, despite sharing 77% amino acid identity, an overall tetrameric structure,[24,25] and identical individual CRD-mannose binding motifs,[17] these two receptors can differentially augment viral infectivity. For example, DC-SIGN is more effective in augmenting the infectivity of some HIV strains than DC-SIGNR,[18,23] while only DC-SIGNR, but not DC-SIGN, can effectively promote West Nile virus infection.[26] Given their close similarity, such differences must result from their different multivalent binding properties, arising presumably from the different spatial and orientation arrangements of their four CRDs, which have been shown to be flexibly linked to the neck domain.[27] These observations make DC-SIGN/R an ideal pair of model multimeric proteins to investigate how subtle structural differences influence multivalent protein−glycan interactions. Unfortunately, the widely used biophysical techniques (e.g., isothermal titration calorimetry (ITC)[28,29] and surface plasmon resonance (SPR)[30]), although powerful in providing quantitative binding affinities, kinetics, and thermodynamics, cannot reveal the structural information (e.g., binding mode, binding site distance, and orientation), which is key to the design of potent multivalent inhibitors.[1,8,9,11] Therefore, there appears to be a clear capability gap of current methods in dissecting such multivalent lectin−glycan interactions.

Herein, we propose that this capability gap may be addressed by developing a polyvalent glycan-quantum dot (QD-glycan)-based multimodal readout strategy to fully exploit multivalency and QD's unique properties. First, the QD's unique, size-dependent, strong, and stable fluorescence[31−33] can be harnessed for binding quantification via a Förster resonance energy transfer (FRET)-based ratiometric readout.[34−38] As compared to other methods (e.g., SPR and ITC), the QD-FRET readout has the advantages of rapid, separation-free detection in solution, high sensitivity, and a ratiometric readout signal with self-calibration function, making it much less sensitive to instrument noise and signal fluctuation, allowing for highly robust, accurate detection.[34−37] Indeed, the QD-FRET technique has been widely employed to address broad biological and biomedical problems, for example, bio/enzymatic-/intracellular- sensing, immunoassays, cell monitoring, and tracking,[31−46] and more recently to probe multivalent protein−glycan interactions.[47] Second, the solid nanoscale core of the QD can be decorated with polyvalent specific glycan ligands to enhance binding affinity by exploiting multivalency. Third, the QD-protein binding can be directly monitored in solution by dynamic light scattering via binding-induced hydrodynamic size changes. Finally, the high contrast of the QD core in scanning transmission electron microscopy (STEM) can be harnessed to directly visualize binding-induced particle arrangements so as to probe the exact binding mode. Despite extensive research, most QD-FRET work reported so far has only utilized the fluorescence property of the QD; hence the unique multifunctionality of the QD probe has not been fully exploited. For example, using the QD-FRET readout strategy, we have recently found that compact polyvalent monomannose-capped QDs (QD-Man) specifically bind to DC-SIGN, but not to DC-SIGNR. We have also proposed that the four CRDs face upward in DC-SIGN, but point sideways in DC-SIGNR, making the latter unable to bind multivalently (>2) to one QD.[47] However, QD-Man failed to differentiate binding of DC-SIGNR and monovalent CRD (Figure S1),[47] possibly due to the fact that the individual CRD-mannose binding is too weak to measure at low concentrations. Therefore, the overall QD-Man-DC-SIGN/R binding modes remain unclear. Herein, we solved this problem by increasing the individual CRD binding affinity of the glycan displayed on the QD and by developing a novel multimodal readout strategy comprising FRET, hydrodynamic size measurement, and S/TEM imaging to fully exploit the unique multifunctionality of the glycan-QD. We further show that there is a good correlation between the QD's DC-SIGN/R binding affinity and their virus inhibition potency.

RESULTS AND DISCUSSION

Glycan Ligand Design and Synthesis. To increase individual CRD-glycan binding affinity, manno-pyranosyl-α-1,2-manno-pyranose (DiMan) was coupled to the terminal end of the dihydrolipoic acid-oligo(ethylene glycol)-based multifunctional ligands[48,49] (abbreviated as DHLA-EG$_n$-DiMan hereafter, where n = 3 or 11 stands for a uniform linker containing 3 or 11 EG units, respectively) using the route described in Scheme 1. For comparison, their monomannosyl equivalent ligands (i.e., DHLA-EG$_n$-Man, n = 3 or 11) were also synthesized as described previously.[47] Individual DiMan-CRD binding is ∼4 times as strong as that of Man-CRD (K_d ≈ 0.9 versus 3.5 mM),[29] allowing us to investigate how individual CRD-glycan affinity contributes to the overall QD-glycan-DC-SIGN/R multivalent binding.

Briefly, lipoic acid (LA) was first coupled to NH$_2$-EG$_n$-N$_3$ (n = 3 or 11) to form LA-EG$_n$-N$_3$ (step i). It was then reduced to LA-EG$_n$-NH$_2$ by triphenyl-phosphine (step ii), and then coupled to cyclooctyne-COOH to form LA-EG$_n$-cyclooctyne (step iii). Meanwhile, 3,4,6-tri-*O*-acetyl-2-*O*-(2,3,4,6-tetra-*O*-acetyl-α-D-mannopyranosyl)-α-D-mannopyranosyl-trichloroacetimidate was reacted with 2-[2-(2-chloroethoxy) ethoxy]-ethanol to introduce a EG$_2$ linker (step iv), which was then treated with NaN$_3$ to convert the linker terminal chloride group into an azide (step v), and after removal of the acetyl protection groups, the azide-modified glycan (1-azido-3,6-dioxaoct-8-yl-2-*O*-α-D-manno-pyranosyl-α-D-mannopyranoside) was obtained (step vi). After that, the azide-modified glycan was coupled to LA-EG$_n$-cyclooctyne via the Cu-free "click" chemistry to give LA-EG$_n$-glycan (step vii), and reduction by tris(2-carboxyethyl)phosphine (TCEP) gave the desired final DHLA-EG$_n$-glycan ligand. Details of the synthesis procedures and their spectroscopic data are given in the Supporting Information. Each DHLA-EG$_n$-glycan ligand contains three different functional domains: a DHLA for robust chelative QD capping;[48,50] a hydrophilic, flexible EG$_n$ linker for imposing high water-solubility, stability, and resistance against non-specific adsorption as well as for tuning the intersugar spacing; and a terminal glycan for specific protein binding.[47]

Preparation and Characterization of Glycan-QDs. The DHLA-EG$_n$-glycan ligands, after deprotonation by NaOH, were

DOI: 10.1021/jacs.7b05104
J. Am. Chem. Soc. 2017, 139, 11833−11844

Scheme 1. Synthetic Route to DHLA-EG$_n$-DiMan (where n = 3 or 11)[a]

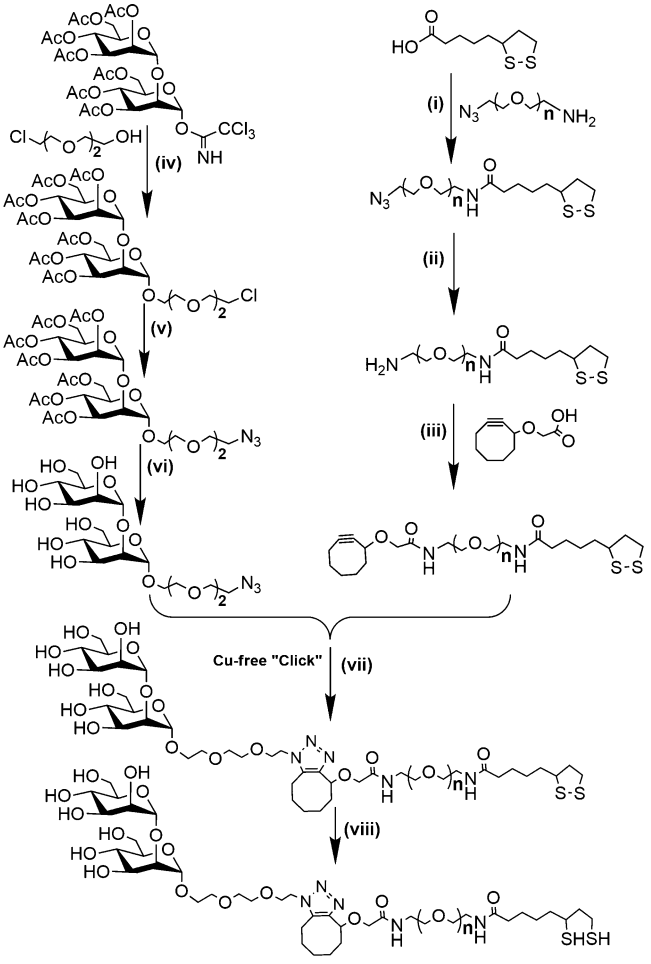

[a]Reaction conditions: (i) DCC/DMAP, DCM; (ii) triphenylphosphine, EtOAc/H_2O; (iii) DCC/DMAP, DCM; (iv) $BF_3{\cdot}OEt_2$, DCM, molecular sieves; (v) NaN_3/TBAI, DMF; (vi) NaOMe, MeOH, then Amberlite H^+ resin; (vii) EtOH; (viii) TCEP·HCl, $CHCl_3$/EtOH/H_2O.

directly used to initiate cap-exchange with a commercial hydrophobic CdSe/ZnS QD (λ_{EM} ≈ 560 nm) in a homogeneous solution using our recently developed highly efficient cap-exchange method.[47] Details of the cap-exchange procedures were given in the Supporting Information section 3. All of the resulting DHLA-EG$_n$-glycan capped QDs (abbreviated as QD-EG$_n$-glycan hereafter) formed highly stable dispersions in aqueous media, and displayed no noticeable changes in appearance or fluorescence over times >1 month. Moreover, the QDs were compact and uniform in size, displaying a small hydrodynamic diameter (D_h) of 8.3 and 9.5 nm for QD-EG$_3$-DiMan and QD-EG$_{11}$-DiMan, respectively (Figure S2),[51] suggesting the formation of isolated, aggregation-free QD dispersions.[52−55] Importantly, the QDs were densely capped with the glycan ligands (glycan valency >220), which would be difficult to achieve by other methods (e.g., post cap-exchange chemical coupling). Using the D_h values and corresponding glycan valencies, the average interglycan distances (d) of the QD-EG$_n$-glycans were estimated in the range of 0.9−1.3 nm (Table 1; see Supporting Information section 6.1 for calculation method). Interestingly, this distance matches well to the average interglycan sequon distance (~1.2 nm) found on the HIV surface heavily glycosylated glycoprotein, gp120.[56,57] Moreover, the QD surface glycan density and interglycan distance (d) can be readily tuned by varying the linker length and diluting the DHLA-EG$_n$-glycan ligand using an inert hydrophilic spacer ligand, DHLA-zwitterion, during the cap-exchange process (see Figure 1).

Differentiating QD-DiMan-DC-SIGN/R Binding Modes by FRET. The DC-SIGN/R proteins were expressed and labeled with an Atto-594 dye at a site-specifically introduced cysteine residue on the CRD (Supporting Information section 4).[47] The chosen mutation residue (Q274 in DC-SIGN and R287 in DC-SIGNR) is located out with the glycan binding sites, minimizing any possible interference with CRD glycan binding. The QD emission has good overlap with the Atto-594 absorption, ensuring that efficient FRET can occur (Förster radius R_0 = ~4.0 nm, Figure S3), but has minimal overlap of dye emission spectra, allowing for easy separation of the QD and dye FRET signal without the need of spectral deconvolution. We first screened the QD-glycan-DC-SIGN/R binding by titrating different amounts of labeled proteins into a fixed concentration of the QD-glycan (40 nM) in a binding buffer (20 mM HEPES, 100 mM NaCl, 10 mM $CaCl_2$, pH 7.8). The resulting fluorescence spectra were shown in Figure 2 (all spectra have been corrected by dye direct excitation background). Similar to QD-Man, incubation of QD-DiMan with the labeled DC-SIGN resulted in significant quenching of QD fluorescence (λ_{EM} ≈ 554 nm) and a concurrent enhancement of the Atto-594 FRET signal (λ_{EM} ≈ 626 nm), consistent with a QD-sensitized Atto-594 FRET mechanism (Figure 2). Moreover, the FRET signal was found to be strongly Ca^{2+}-dependent and was completely diminished in the absence of Ca^{2+} (Figure S4). This observation is fully consistent with the Ca^{2+}-dependency of the DC-SIGN-glycan binding.[17,24] Despite such similarities, three major differences between QD-DiMan and QD-Man binding to DC-SIGN/R were observed:

(1) Most significantly, binding of DC-SIGNR to QD-DiMan produced notable FRET signals, which were markedly higher and well-separated from those of the monovalent CRDs (Figure 2 and Figure S5), a sharp contrast to that of QD-Man where signals obtained from DC-SIGNR and monovalent CRD binding were equally weak and indistinguishable from non-specific adsorption background (Figure S1).[47] Moreover, the apparent FRET ratios (I_{626}/I_{554}) obtained from the monovalent CRD-QD-DiMan binding were still indistinguishable from the background, suggesting that monovalent binding is too weak

Table 1. Summary of the Chemical and Physical Parameters of the QD-EG$_n$-glycan Conjugates

QD surface ligands	glycan valency	D_h (nm)	interglycan spacing (nm)	glycan footprint on QD surface (nm^2)
DHLA-EG$_3$-Man	330 ± 70	8.9 ± 0.1	0.98 ± 0.11	0.75 ± 0.16
DHLA-EG$_{11}$-Man	222 ± 62	9.6 ± 0.2	1.29 ± 0.36	1.30 ± 0.36
DHLA-EG$_3$-DiMan	369 ± 38	8.3 ± 0.1	0.86 ± 0.09	0.59 ± 0.06
DHLA-EG$_{11}$-DiMan	281 ± 25	9.5 ± 0.1	1.13 ± 0.10	1.01 ± 0.09

DOI: 10.1021/jacs.7b05104
J. Am. Chem. Soc. 2017, 139, 11833−11844

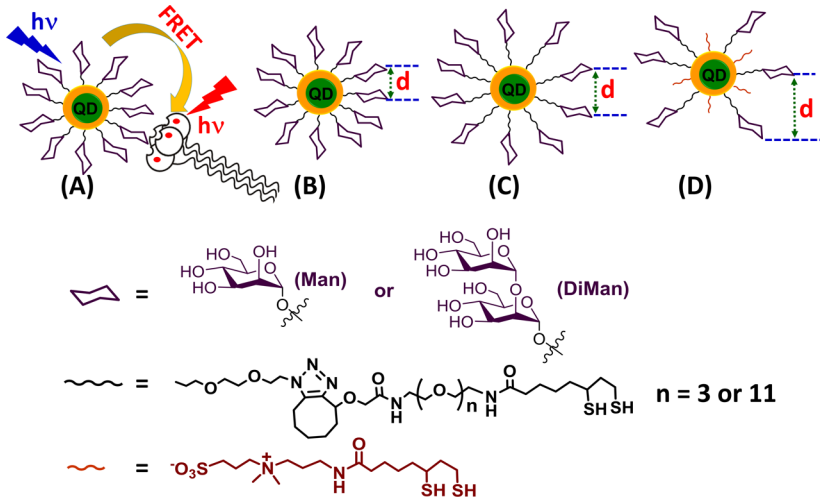

Figure 1. (A) Schematic showing our approach to quantify QD-glycan-DC-SIGN/R multivalent binding by QD-sensitized dye FRET mechanism. (B–D) Schematic presentation of tuning the QD surface glycan valency and interglycan distance (d) via EG linker length (n = 3 for B; n = 11 for C) and glycan dilution with an inert DHLA-zwitterion spacer ligand (D).

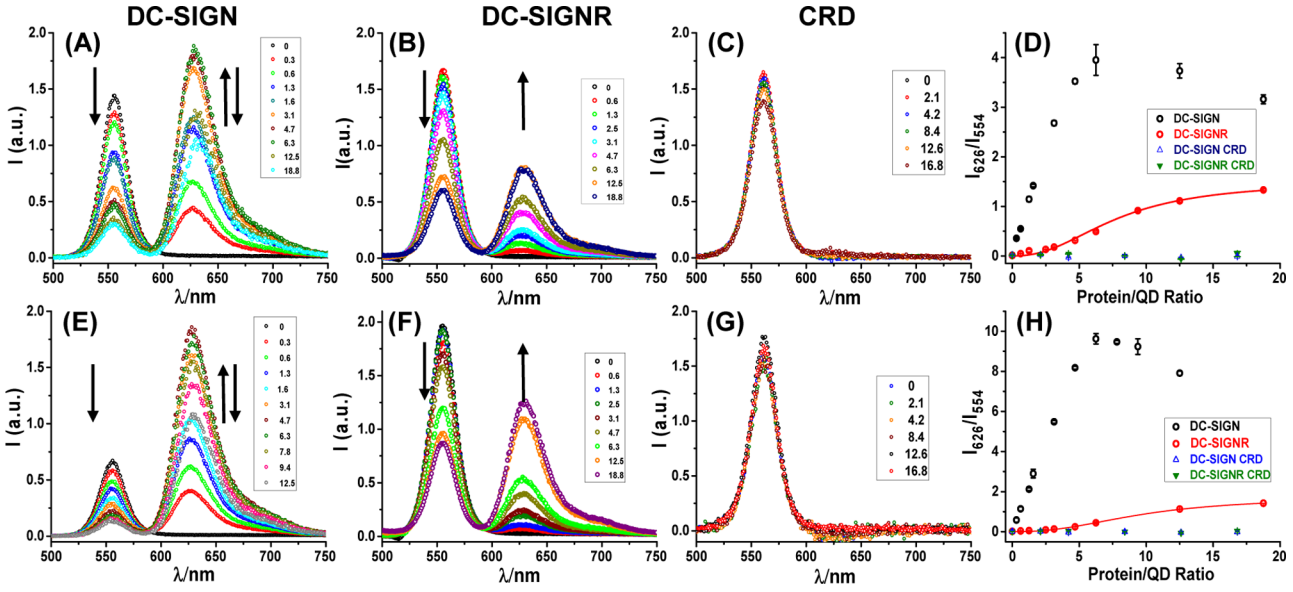

Figure 2. Dye-direct excitation background-corrected fluorescence spectra of QD-DiMan (100% glycan density) after binding to Atto-594-labeled proteins at different protein:QD ratios (PQR): QD-EG_{11}-DiMan + DC-SIGN (A); QD-EG_{11}-DiMan + DC-SIGNR (B); QD-EG_{11}-DiMan + DC-SIGN CRD (C); QD-EG_3-DiMan + DC-SIGN (E); QD-EG_3-DiMan + DC-SIGNR (F); QD-EG_3-DiMan + DC-SIGN CRD (G); and the resulting I_{626}/I_{554} ratio versus PQR relationship for QD-EG_{11}-DiMan (D) and QD-EG_3-DiMan (H). DC-SIGNR binding data are fitted by Hill's equation, $y = R_{max} \times x^n/(k^n + x^n)$, where R_{max} is the maximum I_{626}/I_{554} ratio, k is the PQR value that gives 50% R_{max}, and n is the Hill coefficient. The best fit parameters are R_{max} = 2.6 ± 0.9, k = 17.2 ± 6.1, n = 1.5 ± 0.1, and R^2 = 0.9984 for QD-EG_{11}-DiMan and R_{max} = 1.7 ± 0.2, k = 9.7 ± 1.5, n = 2.4 ± 0.4, and R^2 = 0.9991 for QD-EG_3-DiMan.

($K_d \approx 0.9$ mM)[29] to measure with 40 nM QD. Given that the I_{626}/I_{554} ratio is linearly correlated to the number of acceptors (proteins) bound to each QD in the absence of other quenching effect (see Supporting Information section 5.4),[47] this result implies that DC-SIGNR-QD-DiMan binding is multivalent, and not monovalent; otherwise similar FRET ratios would have been expected.

(2) Binding of DC-SIGN to QD-DiMan still produced a much stronger FRET signal than that of DC-SIGNR (Figure 2), suggesting that DC-SIGN must display a higher binding multivalency to one QD than DC-SIGNR. These results are not unexpected, and, in fact, they are fully consistent with our proposed QD-DC-SIGN/R binding models.[47] The four side-way facing CRDs in DC-SIGNR may split into two pairs and bind divalently with two different QDs. This binding mode should result in positive binding cooperativity. Fitting the DC-SIGNR binding curves by the Hill's function: $y = R_{max} \times x^n/(k^n + x^n)$, where R_{max} is the maximum I_{626}/I_{554} ratio, k is the protein:QD ratio (PQR) that gives 50% R_{max}, and n is the Hill coefficient, indeed revealed that the n values for both QD-EG_{11}-DiMan (1.5 ± 0.1) and QD-EG_3-DiMan (2.4 ± 0.4) were >1, clearly confirming positive binding cooperatively (Figure 2D/H). In contrast, the four upwardly facing CRDs in DC-SIGN may bind tetravalently to a single QD, which should produce no binding cooperativity ($n \leq 1$). Indeed, a similar Hill's fit of the DC-SIGN binding curves with QD-DiMan with 25% glycan

DOI: 10.1021/jacs.7b05104
J. Am. Chem. Soc. 2017, 139, 11833–11844

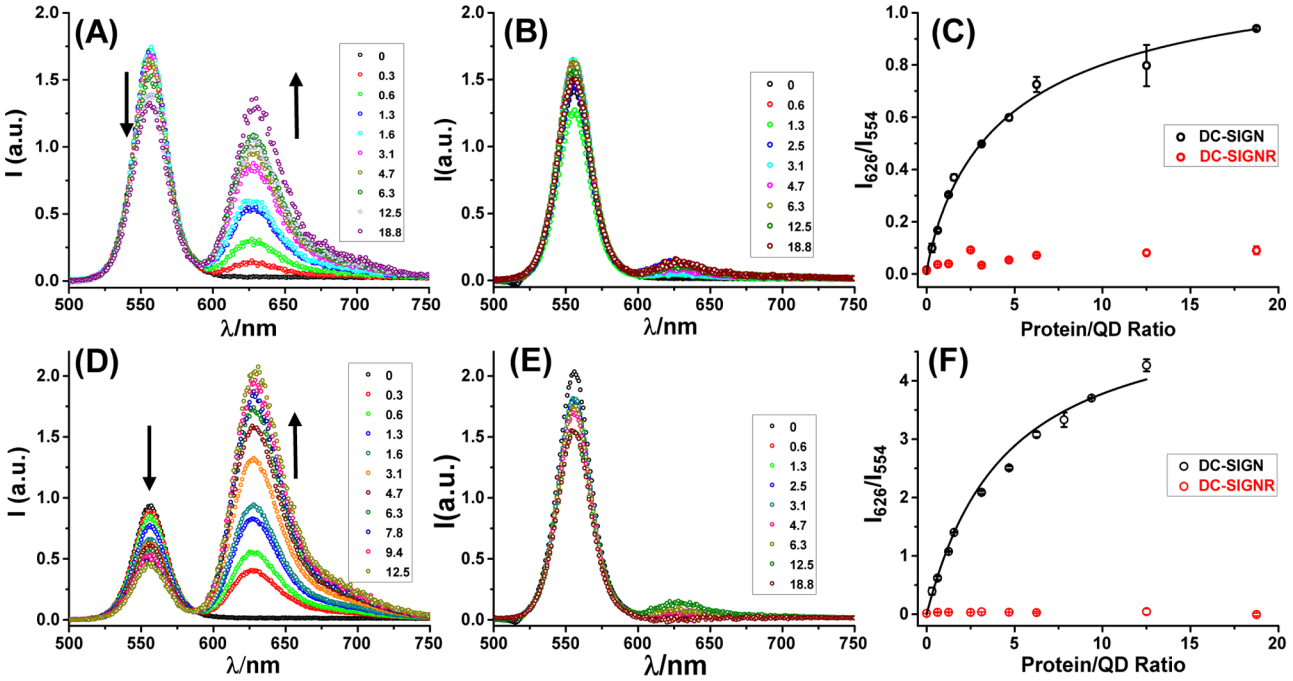

Figure 3. Dye-direct excitation background-corrected fluorescence spectra of QD-EG$_n$-DiMan (with 25% glycan density diluted by DHLA-ZW ligands) after binding to Atto-594-labeled proteins at different PQRs: QD-EG$_{11}$-DiMan + DC-SIGN (A); QD-EG$_{11}$-DiMan + DC-SIGNR (B); QD-EG$_3$-DiMan + DC-SIGN (D); QD-EG$_3$-DiMan + DC-SIGNR (E); and the I_{626}/I_{554} ratio versus PQR relationship for QD-EG$_{11}$-DiMan (C) and QD-EG$_3$-DiMan (F). The DC-SIGN binding data were fitted to Hill's equation, giving R_{max} = 1.2 ± 0.2, k = 4.9 ± 2.1, n = 0.85 ± 0.15, and R^2 = 0.9918 for QD-EG$_{11}$-DiMan and R_{max} = 5.4 ± 1.6, k = 4.4 ± 3.1, n = 1.0 ± 0.3, and R^2 = 0.9994 for QD-EG$_3$-DiMan.

density revealed the n to be 0.85 ± 0.15 for QD-EG$_{11}$-DiMan and 1.0 ± 0.3 for QD-EG$_3$-DiMan, confirming no binding cooperativity (Figure 3). Here, the QD surface glycan density used in DC-SIGN binding was diluted to 25% by DHLA-zwitterion ligand to avoid FRET quenching observed with 100% glycan density QDs at high PQRs (see Figure 2D/H and the next section). Therefore, the different binding multivalency modes of DC-SIGN/R have been successfully differentiated via polyvalent QD-DiMan binding and a ratiometric FRET readout strategy.

(3) Interestingly, unlike the QD-Man-DC-SIGN binding, where the apparent FRET ratio (I_{626}/I_{554}) followed a typical binding pattern with increasing PQR before reaching saturation (Figure S1), the QD-DiMan-DC-SIGN interaction exhibited a distinct two-stage response (Figure 2D/H). The I_{626}/I_{554} ratio initially increased roughly linearly with the PQR at <6 as expected for a single QD-donor in a FRET interaction with N identical receptors model; however, the I_{626}/I_{554} ratio then decreased with the increasing PQR at >6. Using the surface areas calculated from the D_h's of the QDs and the DC-SIGN head footprint, the number of DC-SIGN molecules that can be packed onto the QD surface without crowding was estimated as ~6/~8 for QD-EG$_3$-DiMan/QD-EG$_{11}$-DiMan, respectively (Figure S6). These numbers approximately match the critical PQR (the turning point on the FRET response curve), suggesting that surface crowding is responsible for the observed FRET decrease. The quenching is likely due to crowding-induced reorganization of the QD-bound DC-SIGNs via their flexible neck region[27] that brings the dyes in proximity to each other and causes mutual quenching. This assignment was supported by that no quenching was observed for the labeled DC-SIGN only under equivalent concentrations in the absence of QD-DiMan (Figure S7). Consistent with these results, the fluorescence lifetime of the QD-EG$_{11}$-DiMan (14.75 ns) was reduced to 7.75 ns and further to 1.76 ns as PQR increased from 3 to 10. Meanwhile, the dye lifetime (3.48 ns for protein only) was increased to 8.09 ns at PQR = 3, but then decreased to 4.00 ns at PQR = 10 (Figure S8).[58] Interestingly, diluting the QD surface DHLA-EG$_n$-glycan density to 25% with DHLA-ZW removed the two-stage behavior, and the binding curves returned to their normal shape without FRET quenching at high PQRs (Figure 3C/F). However, it also produced significantly lower (~4-fold) FRET ratios at saturation (Figure 3C/F), suggesting a significantly reduced DC-SIGN binding capacity for the 25% glycan-QD. This result further supports the proposal of surface crowding-induced CRD reorganization being responsible for the FRET quenching observed with the 100% glycan-QDs under high PQRs.

Using the FRET efficiency obtained from the QD quenching (e.g., $E = 1 - I/I_0$, where I and I_0 are the fluorescence intensities of the QD with and without the protein, respectively) and a single QD in FRET interaction with N identical acceptor model, $E = 1/[1 + (r/R_0)^6/N]$,[34] the average QD-dye distance r was calculated to be ~5.2 and ~5.7 nm for DC-SIGN binding to QD-EG$_3$-DiMan and QD-EG$_{11}$-DiMan, respectively (Figure S3C and D). Both r values were ~1 nm longer than the hydrodynamic radii of the corresponding QD-EG$_n$-glycans (e.g., ~4.2 and ~4.8 nm). This result is not unreasonable considering the distance between the dye labeling position and the glycan binding site, as well as the flexible nature of the EG$_n$ linker, which may become more extended upon protein binding. However, the equivalent FRET efficiency versus dye:QD ratio responses for DC-SIGNR binding to QD-DiMan were S-shaped and could not be fitted by the single QD in FRET interaction with N identical acceptor model (Figure S3C/D). The relatively weak binding between DC-SIGNR and

DOI: 10.1021/jacs.7b05104
J. Am. Chem. Soc. 2017, 139, 11833−11844

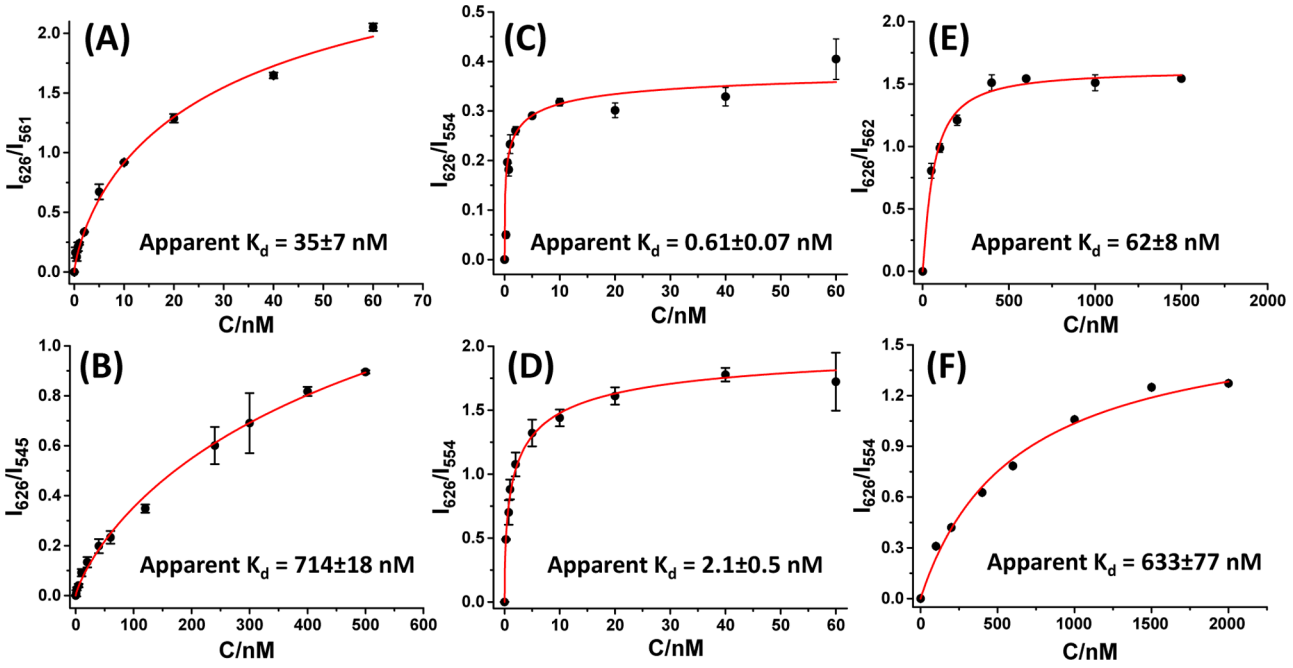

Figure 4. Relationship between the I_{626}/I_{554} ratio and protein concentration for a fixed protein:QD molar ratio of 1:1 for DC-SIGN and 10:1 for DC-SIGNR. (A) DC-SIGN + QD-EG$_3$-Man; (B) DC-SIGN + QD-EG$_{11}$-Man; (C) DC-SIGN + QD-EG$_3$-DiMan; (D) DC-SIGN + QD-EG$_{11}$-DiMan; (E) DC-SIGNR + QD-EG$_3$-DiMan; and (F) DC-SIGNR + QD-EG$_{11}$-DiMan. Data were fitted by Hill's equation, $Y = R_{max} \times C^n/[K_d^n + C^n]$, where R_{max}, K_d, n, and C are the maximum I_{626}/I_{554} ratio, apparent K_d, Hill coefficient, and protein concentration, respectively. The fitting parameters were summarized in Table S1.

Table 2. Key Chemical and Biophysical Parameters of the QD-EG$_n$-glycans and Their Binding Affinities with DC-SIGN/R Measured by FRET

QD surface ligands	glycan valency (N)	apparent $K_{d\ DC\text{-}SIGN}$ (nM)	apparent $K_{d\ DC\text{-}SIGNR}$ (nM)	enhancement factor β[a]	β/N
DHLA-EG$_3$-Man	330 ± 70	35 ± 7		100 000	~300
DHLA-EG$_{11}$-Man	222 ± 62	714 ± 18		4900	~22
DHLA-EG$_3$-DiMan	369 ± 38	0.61 ± 0.07	62 ± 8	1 480 000	~4000
DHLA-EG$_{11}$-DiMan	281 ± 25	2.1 ± 0.5	633 ± 77	430 000	~1500

[a]DC-SIGN affinity enhancement factor is calculated by $\beta = K_{d\ (CRD\text{-}Glycan)}$/Apparent $K_{d(DC\text{-}SIGN\text{-}QD)}$, where $K_{d\ CRD\text{-}Man}$ and $K_{d\ CRD\text{-}DiMan}$ are 3.5 and 0.9 mM, respectively.[29]

QD-DiMan (>100-fold weaker than that of DC-SIGN equivalent, see the next section) and positive binding cooperatively may have led to the S-shape response curve, presumably because DC-SIGNR added under low PQRs was unable to bind efficiently to QD-DiMan to produce efficient FRET at the early stages of titration.

Quantifying QD-glycan-DC-SIGN/R Binding Affinity by FRET. The different QD-binding modes and multivalency exhibited by DC-SIGN/R should result in differing binding affinities (K_d's). Theoretically, the I_{626}/I_{554} ratio is linearly correlated to the numbers of acceptors (proteins) bound to the QD, making it a reliable signal for quantifying the proportion of the bound QD-protein complexes in a QD/protein mixture (Supporting Information section 5.4).[47,59] Here, we have developed a new method by simultaneously changing the QD/protein concentration while keeping PQR fixed at 1 for DC-SIGN (to avoid the FRET quenching at high PQRs) or 10 for DC-SIGNR (to compensate the low FRET ratio at PQR = 1, Figure S9). Under such conditions, the I_{626}/I_{554} intensity ratio can provide a true reflection of the fraction of bound QD-protein complexes within the QD-protein mixture. The experiments were performed in the binding buffer containing 1 mg/mL of bovine serum albumin (BSA) to minimize the possible nonspecific adsorption of QD/protein on surfaces, which were non-negligible at low concentrations (<10 nM).[59] The resulting fluorescence spectra revealed that both the dye FRET and the QD fluorescence signals increased with the increasing concentration (Figure S9). However, the former increased faster than the latter, giving an increased I_{626}/I_{554} ratio with the increasing concentration. The resulting I_{626}/I_{554} ratio−concentration relationships were fitted by the Hill's equation to derive the apparent dissociation constants (K_d's, Figure 4). The parameters derived from the best fits were summarized in Table 2.

Four notable findings are revealed by Table 2. First, a polyvalent display of DiMan on the QD greatly enhanced its affinity for DC-SIGN: a remarkably low apparent K_d of 610 pM was achieved with QD-EG$_3$-DiMan, translating to a massive ~1.5 million-fold affinity enhancement (β) over the monovalent CRD-DiMan binding ($K_d \approx 0.9$ mM),[29] and a normalized per sugar enhancement factor, β/N, of ~4000. Second, although a polyvalent display of Man on the QD also enhanced its DC-SIGN affinity, the level of enhancement was significantly lower than that of the DiMan equivalent (<1/10 in β/N terms). This difference may be due to the extended binding surface of the DC-SIGN CRD, which contains both

DOI: 10.1021/jacs.7b05104
J. Am. Chem. Soc. 2017, 139, 11833−11844

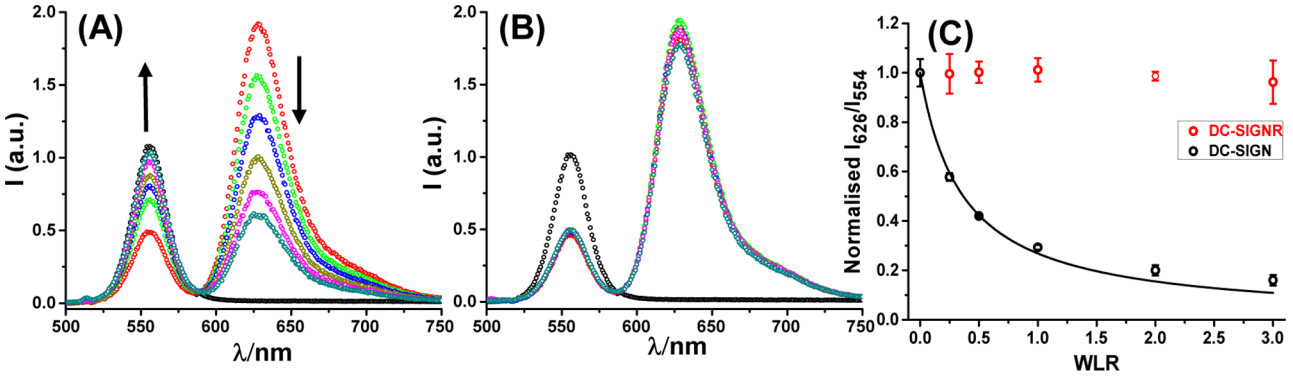

Figure 5. Dye-direct excitation background corrected fluorescence spectra of QD-EG_3-DiMan(25%)/DHLA-ZW(75%) + Atto-594 labeled DC-SIGN (PQR = 12.5 to ensure saturate protein binding) after mixing with different amounts of wild-type DC-SIGN (A) or DC-SIGNR (B). The QD-only fluorescence spectra in the absence of proteins are also displayed for comparison (shown in ○). (C) Plots of the corresponding normalized I_{626}/I_{554} ratio versus wild-type protein:labeled DC-SIGN molar ratio (WLR) fitted by a competitive binding model.

primary and secondary binding sites.[17,24] For QD-Man, it may bind mainly to the primary site, whereas QD-DiMan may bind to both primary and secondary sites, leading to greater affinity enhancement. Third, the apparent K_d for QD-DiMan binding to DC-SIGN was found to be >100-fold lower than that to DC-SIGNR, suggesting that DC-SIGN's binding affinity is >100-fold stronger than that of DC-SIGNR. Given that each HIV surface gp120 trimer spike is densely coated with mannose containing glycans[57] and is of size (~12 nm)[60] comparable to a QD-DiMan, this result thus provides a plausible explanation why DC-SIGN has been found to be more effective in trans-infecting some HIV strains than DC-SIGNR.[23] Moreover, this result explains the reason why wild-type DC-SIGNR was unable to compete off DC-SIGN from binding to QD-DiMan observed in the next section. Finally, the flexible EG linker also had a significant impact on the overall binding affinity: increasing the linker length from 3 to 11 EG units led to >3-fold lower affinity. This is presumably because the longer is the EG linker the more flexible and disordered the terminal glycans will be, and hence there is a greater entropic penalty to pay upon DC-SIGN binding. Nevertheless, a suitable EG linker is essential to impose high QD stability in aqueous media and to minimize nonspecific interactions with nontarget proteins.

Confirming QD-DC-SIGN/R Binding Specificity Using Wild-Type Receptor Competition. A FRET competition experiment using unlabeled wild-type proteins was further employed to confirm that the labeled DC-SIGN/R (containing a site-specific cysteine mutation and Atto-594 labeling, see Supporting Information section 4)-QD binding truly reflected wild-type protein binding properties. The experiment was performed on the QDs with 25% glycan density to overcome the FRET quenching problem observed with 100% glycan-QD (Figure S10A). As the wild-type protein:labeled DC-SIGN ratio (WLR) increased, the FRET signal reduced progressively while the QD fluorescence correspondingly recovered (Figure 5A), confirming that wild-type DC-SIGN successfully displaced labeled DC-SIGNs from binding to the QD. In contrast, wild-type DC-SIGNR caused no apparent changes to either the QD or the FRET signal (Figure 5B), suggesting no binding competition occurred. These results indicate that wild-type and labeled DC-SIGN molecules must bind to the same sugar sites (same binding mode) on the QD surface, whereas DC-SIGNR may be too weak to displace the labeled DC-SIGN from binding to the QD. Their different competition efficiencies were clearer in the normalized I_{626}/I_{554} versus WLR plots (Figure 5C), where DC-SIGNR gave no apparent changes but DC-SIGN yielded significantly reduced FRET ratios. This result is not unexpected because DC-SIGNR-QD-DiMan binding is >100-fold weaker than that of the equivalent DC-SIGN interaction (see previous section, Table 2).

The relative affinity between wild-type and labeled DC-SIGN for the QD-DiMan binding was further evaluated by a simple competitive model, $F = IR_{50}/[IR_{50} + C_{WT}/C_{LP}]$, where F is the FRET ratio in the presence of wild-type protein normalized by that without, C_{WT} and C_{LP} are wild-type and labeled protein concentrations, respectively, and IR_{50} is the molar ratio of wild type DC-SIGN:labeled DC-SIGN required to reduce F by 50%. An IR_{50} value of 1 indicates that both proteins bind to the QD with equal affinity, while an IR_{50} value of <1 indicates that the labeled protein binds more weakly than wild-type protein. Fitting the data using this model gave an IR_{50} value of 0.88 and 0.37 for QD-EG_{11}-DiMan and QD-EG_3-DiMan, respectively (Figure 5 and Figure S10). Both IR_{50} values were <1, indicating that the site-specific mutation and dye-labeling in DC-SIGN weakened its binding affinity with the QDs. This effect was more pronounced for QD-EG_3-DiMan, presumably because its shorter EG_3 linker may limit the terminal sugar's ability to reorganize and fit perfectly within the protein's binding pockets.

Differentiating QD-Wild-Type Protein Binding Modes by DLS, TEM, and Fluorescence Quenching. The hydrodynamic size (D_h) of the QD-protein assemblies provided further support for the different binding modes of DC-SIGN/R.[51] Binding of wild-type DC-SIGN with QD-EG_{11}-DiMan (PQR = 12.5) gave only a single, narrowly distributed species with a D_h of ~42 nm (Figure 6B). This value was significantly bigger than that of isolated QDs ($D_h \approx 8.8$ nm in binding buffer, Figure 6A) or wild-type DC-SIGN ($D_h \approx 14$ nm, Figure S11), suggesting that all DC-SIGNs were bound to the QD and formed a uniform QD-protein assembly. In contrast, binding of wild-type DC-SIGNR gave a bimodal distribution with D_h's of ca. 124 and 205 nm (Figure 6C), respectively. Moreover, almost identical D_h distributions were also observed with its equivalent QD-EG_3-DiMan interaction (Figure S2D, Table S2). These D_h values were too large to be isolated as individual QD-protein assemblies, a strong indication of QD agglomeration via QD/DC-SIGNR interlinking. This hypothesis was confirmed by two-dimensional imaging of the QD dispersions via rapid plunge freezing and subsequent TEM/STEM imaging at low magnification after analytical confirmation of the QD size and contrast level in these images[61] (we term this cryo-snapshot

DOI: 10.1021/jacs.7b05104
J. Am. Chem. Soc. 2017, 139, 11833−11844

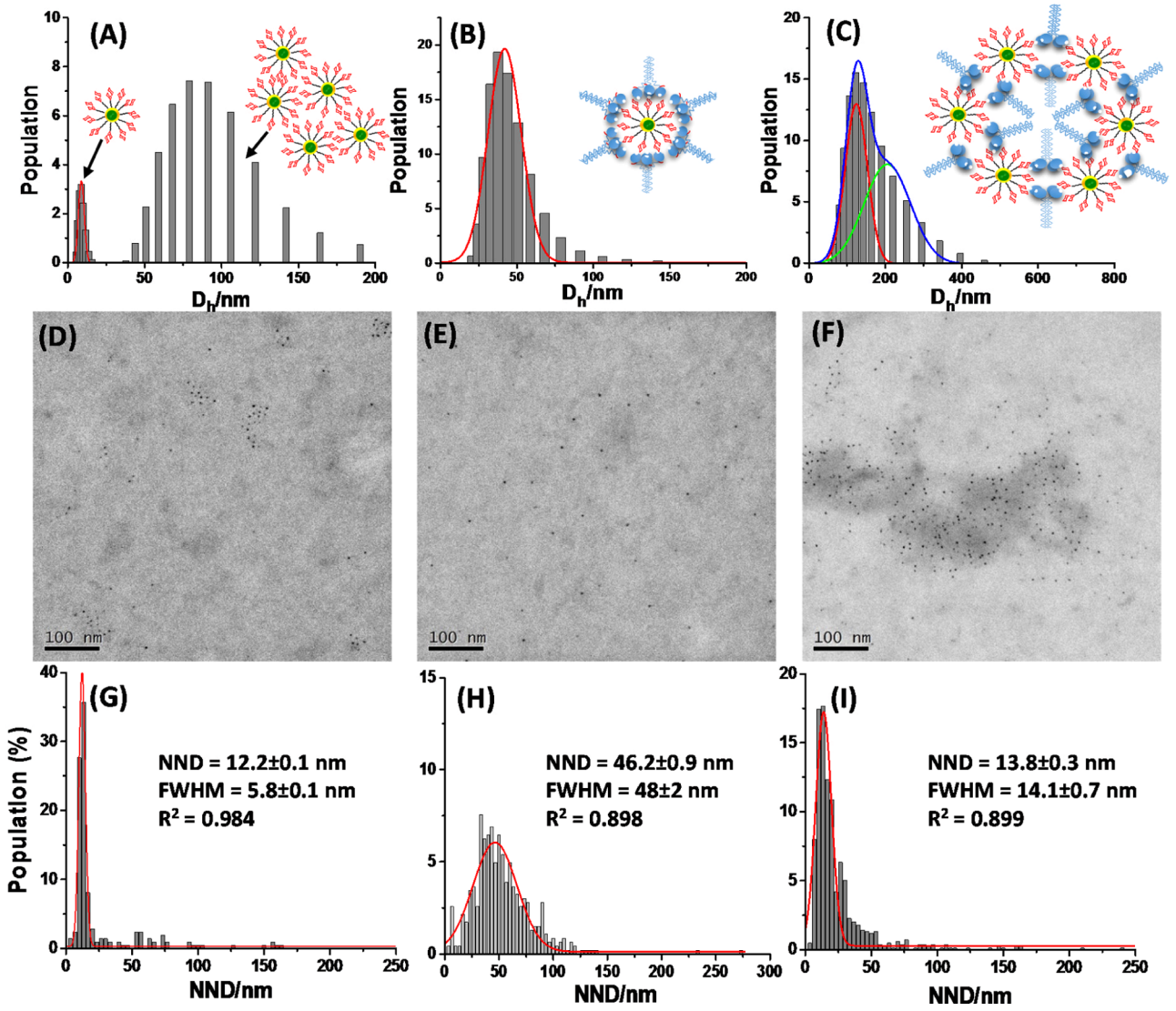

Figure 6. Hydrodynamic diameter histograms of QD-EG_{11}-DiMan before (A) and after binding to wild-type DC-SIGN (B) or DC-SIGNR (C) measured by dynamic light scattering (DLS). Insets show schematics of the QD and/or QD-protein assemblies. Cryo-TEM (contrast inverted HAADF STEM) images of the QD-EG_{11}-DiMan before (D) and after binding to wild-type DC-SIGN (E) or DC-SIGNR (F). Consistent with the D_h values shown in (A), both isolated and clustered QDs are found in the corresponding TEM image (D) for QD-EG_{11}-DiMan. Histograms of nearest neighbor distance (NND) distributions measured from the TEM images of QD-EG_{11}-DiMan before (G) and after binding to wild-type DC-SIGN (H) or DC-SIGNR (I). The distribution histograms were fitted by Gaussian function with fitting parameters shown in each graph. All samples were measured in binding buffer.

TEM/STEM, SI section 6), where the high contrast of the QD was employed as the differentiating modality. Figure 6D shows that the QDs clustered in the binding buffer, possibly due to weak binding between Ca^{2+} ions and QD-surface DiMan ligands because QD-DiMan appeared as isolated particles in pure water without Ca^{2+} (Figure S12). However, the QD-DiMan clusters were completely dispersed upon binding with wild-type DC-SIGN, revealing only isolated QDs (Figure 6E), whereas binding of wild-type DC-SIGNR produced more aggregated QDs (Figure 6F). The different binding behaviors were further supported by a nearest neighbor particle distance (NND) analysis of TEM images (see Supporting Information section 6).[61] A large NND of ∼46 nm was found for DC-SIGN bound QDs, which was >3 times that of DC-SIGNR bound QDs (∼14 nm) or clustered QDs in binding buffer (∼12 nm, see Figure 6G/H/I). These results agree excellently with the DLS results and our proposed DC-SIGN/R binding modes. The strong tetravalent binding of DC-SIGN with one QD should produce isolated QDs, preventing them from getting close to each other and hence a large NND, whereas the bis-divalent binding of DC-SIGNR with two different QDs should lead to QD interlinking and a small NND.

The postulated DC-SIGN/R-QD binding modes were further supported by the different fluorescence quenching behaviors by DHLA-EG_3-DiMan coated gold nanoparticles (GNP-EG_3-DiMan, Figure S13). GNP was chosen here because its efficient universal fluorescence quenching can extend beyond the traditional FRET distance limit of ∼10 nm.[62,63] Here, a 605 nm emitting QD was used to minimize the QD fluorescence reduction due to absorption of GNP at the excitation wavelength (λ_{EX} = 590 nm). Mixing GNP-EG_3-DiMan (5 nM) with QD-EG_3-DiMan (10 nM) in binding buffer gave almost the same fluorescence as the QD alone, suggesting minimal QD-GNP cross-linking. Addition of wild-

DOI: 10.1021/jacs.7b05104
J. Am. Chem. Soc. 2017, 139, 11833−11844

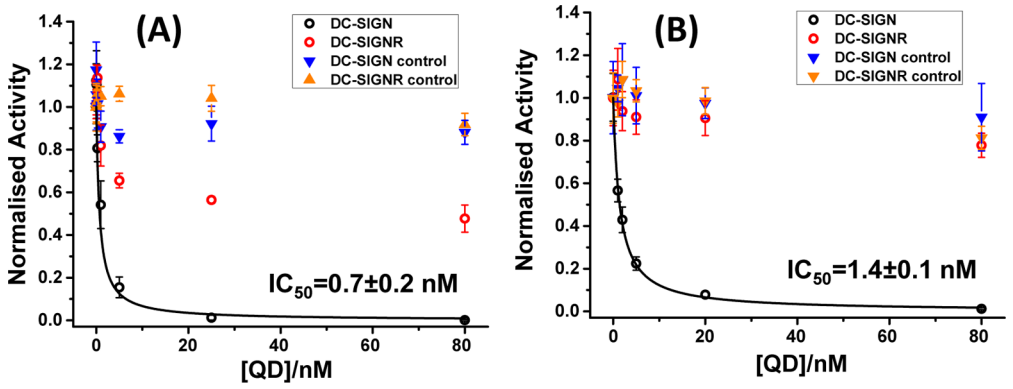

Figure 7. Normalized luciferase activities of the DC-SIGN- or DC-SIGNR-expressing 293T cells as a function of the pretreatment QD-EG_3-DiMan (A) or QD-EG_{11}-DiMan (B) concentration. The data for particles bearing the Ebola virus glycoprotein (EBOV-GP) are shown in open circles, while the results obtained with control particles bearing the vesicular stomatitis virus glycoprotein (VSV-G) are shown in triangles. The luciferase activities, after subtraction by their corresponding pcDNA control background, were normalized by the respective values in the absence of the QDs (Figure S15). Data were fitted by a competitive binding model, $F = IC_{50}/(IC_{50} + C_{QD})$, where F is the normalized luciferase activity, C_{QD} is the QD concentration, and IC_{50} is the concentration that gives 50% inhibition.[47] The gene transduction driven by a control vector bearing VSV-G, which cannot use DC-SIGN/R to augment cell entry, was unaffected by the QD treatment, confirming that the specific QD-DC-SIGN/R binding was responsible for the observed inhibition.

type DC-SIGNR to the QD-GNP mixture significantly quenched the QD fluorescence, whereas introduction of wild-type DC-SIGN increased the QD fluorescence considerably (Figure S14). These results matched well to that expected from the DC-SIGN/R binding modes: cross-linking by DC-SIGNR should lead to QD/GNP assembly and QD fluorescence quenching by the proximal GNPs, whereas the strong tetravalent binding of DC-SIGN to one QD or GNP should not only prevent any GNP or QD assembly, but also break up any preassembled QD clusters in binding buffer (see Figure 6D), resulting in higher fluorescence over the QD-only sample.

Inhibiting DC-SIGN/R-Mediated Augmentation of EBOV-GP-Driven Viral Entry. The strong DC-SIGN binding affinity afforded by QD-EG_n-DiMan suggests that these QDs could effectively block DC-SIGN-mediated virus infection. To investigate this potential, a murine leukemia virus (MLV)-based vector bearing the EBOV-GP was employed to deliver the luciferase gene into human embryonic kidney cells (293T) previously transfected to express DC-SIGN/R.[47] The virus particles can bind to cell surface DC-SIGN/R via incorporated EBOV-GPs on their membrane surface to enhance cell uptake and gene transduction. As expected, DC-SIGN/R expression in cells greatly increased the efficiency of EBOV-GP-driven gene transduction. Pretreatment of cells with QD-EG_n-DiMan greatly reduced the gene transduction of DC-SIGN-positive cells down to the low nanomolar range, indicating high inhibition potency (Figure S15). The normalized inhibition data were fitted by an inhibition model, giving an IC_{50} of 0.7 ± 0.2 and 1.4 ± 0.1 nM for QD-EG_3-DiMan and QD-EG_{11}-DiMan, respectively (Figure 7). Such low IC_{50} values place them among the most potent glyconanoparticle inhibitors against EBOV-GP-driven transduction of host cells. In fact, their inhibition potency is comparable to those of the giant globular multivalent glycofullerenes (IC_{50} = 0.667 nM)[14] and the virus-like glycodendri-nanoparticles (IC_{50} = 0.91 nM).[13]

Interestingly, these IC_{50} values roughly matched their apparent binding K_d's with DC-SIGN (i.e., 0.61 and 2.1 nM) measured by QD-FRET (Table 2). Moreover, the gene transduction of DC-SIGNR-expressing cells was reduced only marginally by treatment with 80 nM QD-EG_{11}-DiMan (~10%), but it was more pronounced with QD-EG_3-DiMan (~50%). The inhibition potencies obtained here again roughly matched those expected from their respective DC-SIGNR binding apparent K_d's (i.e., ~633 and ~62 nM) measured by FRET. The good match between the apparent K_d and IC_{50} values demonstrated that our FRET-based K_d measurement could serve as a viable, rapid method for predicting virus inhibition potency of glyconanoparticles at the cellular level. Although the toxic cadmium content can prevent the current QD-glycans from being used for treatment and prevention of EBOV infection, replacing the CdSe/ZnS QD with other biocompatible, nontoxic nanoparticles (e.g., gold, Cd-free QD) should overcome this problem, where nanoparticles displayed with similar polyvalent glycan ligands could be used as potent, specific virus inhibitors and therapeutic reagents.

CONCLUSIONS

We have demonstrated that compact QDs displaying dense polyvalent DHLA-EG_n-DiMan ligands are powerful probes for dissecting multivalent protein−glycan interactions via multimodal readout strategies (FRET, particle size analysis, TEM imaging, and GNP-based fluorescence quenching). Unlike most other glycoconjugates that were constructed on passive scaffolds, the unique properties of QD (e.g., fluorescence, size, and inherent TEM contrast) have been fully exploited for the purpose of multimodal readout for the first time. Significantly, we have revealed that DC-SIGN binds tetravalently to a single QD, whereas DC-SIGNR binds divalently to two different QDs. The different binding modes, arising from the different CRD spatial arrangements, yield >100-fold tighter QD-DiMan binding affinity for DC-SIGN over DC-SIGNR, which also help to explain why DC-SIGN is more effective in trans-infecting some HIV strains than DC-SIGNR. Moreover, a new QD-FRET-based ratiometric method has been developed to quantify the apparent QD-protein binding K_d. An impressively low K_d (~610 pM) and a per glycan affinity enhancement factor (β/N) of ~4000 have been attained with QD-DiMan. Importantly, QD-DiMan was found to potently inhibit DC-SIGN-mediated augmentation of EBOV-GP-driven infection of host cells with an IC_{50} of ~0.7 nM, placing it among the most potent inhibitors against the EBOV-GP driven virus infections.[10,13,14] Moreover, this IC_{50} value also matches

DOI: 10.1021/jacs.7b05104
J. Am. Chem. Soc. 2017, 139, 11833−11844

well to its DC-SIGN binding apparent K_d measured by the ratiometric QD-FRET readout strategy. Together, these results demonstrate that the QD-FRET-based affinity measurement developed herein could serve as a robust, rapid, and sensitive method for predicting glyconanoparticle inhibition potencies against EBOV-GP driven virus infections at the cellular level.

EXPERIMENTAL SECTION

Materials. A CdSe/ZnS core/shell QD ($\lambda_{EM} \approx 560$ nm) was purchased from PlasmaChem GmbH (Berlin, Germany). The QD was supplied as dry powders and capped with mixed ligands of trioctylphosphine oxide (TOPO), hexadecylamine, and oleic acid. A CdSe/ZnSe/ZnS core/shell/shell QD capped with mixed ligands of TOPO and trioctylphosphine ($\lambda_{EM} \approx 605$ nm) in toluene was purchased from STREM chemicals UK Ltd. *O*-(2-Aminoethyl)-*O*′-(2-azidoethyl)decylethylene glycol (N_3-EG_{11}-NH_2, >95% oligomer purity) was purchased from Polypure Plc (Norway). Azido-3,6,9-trioxyundecan-1-amine (N_3-EG_3-NH_2, >90% monomer purity), *N*,*N*-dimethyl-1,3-propanediamine (>99%), 1,3-propane-sultone (>99%), lipoic acid (LA, >99%), triphenylphosphine (>98.5%), dicyclohexylcarbodiimide (DCC, >99%), dimethylamino-pyridine (DMAP, >99%), tris(2-carboxyethyl)phosphine hydrochloride (TCEP·HCl, >98%), and other chemicals were purchased from Sigma-Aldrich UK Ltd. (Dorset, UK). Solvents were obtained from Fisher Scientific (Loughborough, UK). Ultrapure water (resistance >18.2 MΩ cm) purified by an ELGA Purelab classic UVF system was used for all experiments and making buffers.

Preparation of QD-EG_n-glycan (n = 3 or 11).[47] One nanomole of CdSe/ZnS QD in 0.2 mL of toluene was first precipitated by 1 mL of ethanol followed by centrifugation to remove any free ligands. The QD pellet was dissolved in $CHCl_3$ (50 μL), then DHLA-EG_n-glycan ligand (0.80 μmol in $CHCl_3$) predeprotonated by NaOH (8.0 μL, 0.10 M in EtOH) and MeOH were added to make a homogeneous solution ($CHCl_3$:MeOH = 1:1 v/v). The resulting solution was wrapped in aluminum foil and stirred at room temperature (rt) for 30 min. Hexane was then added until the solution became cloudy. The mixture was centrifuged at 10 000*g* for 5 min, where all of the formed QD-EG_n-glycan pelleted. After removal of the clear supernatant, the pellet was dissolved in 100 μL of pure H_2O and transferred to a 30 kDa MWCO spin column and washed with H_2O (3 × 100 μL) to remove any unbound free ligands, yielding the QD-EG_n-glycan stock. The QD concentration was determined by its first exciton peak absorbance at 546 nm ($\varepsilon = 1.3 \times 10^5$ M^{-1} cm^{-1}) using the Beer–Lambert law.[47]

Fluorescence Spectroscopy. All fluorescence spectra were recorded on a Cary Eclipse fluorometer using a fixed excitation wavelength, λ_{EX}, of 450 nm, corresponding to the absorption minimum of Atto-594 to minimize the direct excitation background. The measurements were performed in a binding buffer (20 mM HEPES pH 7.8, 100 mM NaCl, 10 mM $CaCl_2$) containing 10 μg/mL of a His_6-Cys peptide, which we found to improve the QD stability and reduce nonspecific adsorption.[47,59] The labeled proteins were mixed with the QD at room temperature for 20 min before fluorescence spectra were recorded. Binding of labeled monomeric DC-SIGN or DC-SIGNR CRD with the QDs was performed the same way. For apparent K_d measurement, a series of samples containing different concentrations of the QD/labeled proteins (but with a fixed PQR of 1 for DC-SIGN or 10 for DC-SIGNR) were prepared in the same binding buffer as above but containing 1 mg/mL of BSA to reduce nonspecific adsorption. The samples were incubated at room temperature for 20 min before fluorescence spectra were recorded. Adjustments of the PMT voltages and EX/EM slit widths were used to compensate the low fluorescence signal at low concentrations. Although this may affect the absolute fluorescence intensity, the FRET ratio is not affected due to its ratiometric nature. All fluorescence spectra were corrected for the dye direct excitation background by subtracting the corresponding fluorescence spectrum of the same concentration labeled protein only recorded under identical conditions.

Data Fitting. Direct excitation background corrected fluorescence peak intensities at 554 nm (QD) and 626 nm (Atto-594 FRET) were used to calculate the apparent FRET ratio, I_{626}/I_{554}. The I_{626}/I_{554} ratio versus protein concentration plots were fitted to Hill's equation to derive the apparent K_d:

$$I_{626}/I_{554} = (R_{max} \times [C]^n)/(K_d^{\,n} + [C]^n) \quad (1)$$

where R_{max} is the saturated FRET ratio, K_d is the apparent dissociation constant, $[C]$ is the protein concentration, and n is Hill's coefficient. Iterative fittings were used to yield the best fit (R^2) for R_{max} and K_d determination. The relative binding affinity between wild-type and labeled DC-SIGN for the QD-DiMan was analyzed by a simple competitive model, $F = IR_{50}/[IR_{50} + C_{WT}/C_{LP}]$, where F is the apparent FRET ratio in the presence of wild-type protein normalized by that without, and C_{WT} and C_{LP} are wild-type and labeled protein concentrations, respectively. Iterative fittings were used to yield the best fit (R^2) for the IR_{50} determination.

STEM Imaging. Three QD samples (QD-EG_{11}-DiMan, QD-EG_{11}-DiMan + wild-type DC-SIGN, and QD-EG_{11}-DiMan + wild-type DC-SIGNR) were prepared in binding buffer with C_{QD} = 40 nM and $C_{protein}$ = 1.5 μM. 3.5 μL of the QD sample was placed onto a plasma-cleaned TEM grid with a continuous carbon support film, blotted, and plunge frozen into liquid ethane. The TEM grids were then warmed to room temperature over several minutes by placing them in the liquid nitrogen cooled storage container in a rotary pumped vacuum desiccator. The samples were analyzed using an FEI Titan Cubed Themis 300 G2 S/TEM equipped with FEI SuperX energy dispersive X-ray (EDX) spectrometers. The samples were imaged using high angle annular dark field scanning transmission electron microscopy (HAADF STEM) mode,[61,64] which provides atomic number contrast ($\approx Z^{1.7}$), thereby permitting imaging of the high atomic number quantum dots (brighter) on the low atomic number background (darker). A series of images at the same magnification were recorded for each sample, which were then analyzed in MATLAB to measure the nearest neighbor distances (NNDs). Histograms of NNDs for each image were produced. The combined histograms were plotted as a percentage of the total population and fitted by Gaussian distribution.

Inhibition of DC-SIGN/R-Mediated Augmentation of EBOV-GP-Driven Transduction.[47] The experiments were performed using human embryonic kidney 293T cells. Target 293T cells seeded in 96-well plates were transfected with plasmids encoding DC-SIGN or DC-SIGNR or control transfected with empty plasmid (pcDNA). The cells were washed at 16 h post transfection and further cultivated at 37 °C, 5% CO_2 in Dulbecco's modified eagle medium (DMEM) containing 10% fetal bovine serum (FBS). At 48 h post transfection, the cells were exposed to twice the final concentration of QD-DiMan inhibitor in DMEM supplemented with 10% FBS for 30 min in a total volume of 50 μL. Thereafter, the cells were inoculated with 50 μL of preparations of MLV vector particles encoding the luciferase gene and bearing either EBOV-GP or the vesicular stomatitis virus glycoprotein (VSV-G) as control. Binding of QD-DiMan to DC-SIGN/R on the surface of 293T cells can block the interaction of these lectins with the EBOV-GP on the particle surface, reducing the cellular uptake of vector particles and thus reducing transduction efficiency. At 6 h post inoculation, 100 μL of fresh DMEM culture medium was added, and the cells were incubated for another 72 h. Thereafter, luciferase activities in cell lysates were determined using a commercially kit (PJK), following the manufacturer's instructions, as described in our previous publication.[47]

ASSOCIATED CONTENT

Supporting Information

The Supporting Information is available free of charge on the ACS Publications website at DOI: 10.1021/jacs.7b05104.

Experimental details that include the detailed synthesis and spectroscopic characterization of the DHLA-EG_n-DiMan ligands, DC-SIGN/R production, and labeling; lifetime measurement, STEM and DLS measurements,

DOI: 10.1021/jacs.7b05104
J. Am. Chem. Soc. 2017, 139, 11833–11844

calculation of interglycan distance, virus inhibition experiment, supporting tables showing the physical parameters of the QD-EG$_n$-glycan, fitting parameters, and supporting figures showing the hydrodynamic size distributions of the proteins and QDs with and without proteins; QD-Atto594 Förster radius (R_0) and average QD-dye distance (r); Ca^{2+} dependence of DC-SIGN/R QD binding; lifetime decay curves; GNP-DiMan hydrodynamic size and TEM image; QD fluorescence quenching by GNP in the presence of DC-SIGN/R; and original virus inhibition data (PDF)

AUTHOR INFORMATION

Corresponding Authors

*y.guo@leeds.ac.uk
*d.zhou@leeds.ac.uk

ORCID

Dejian Zhou: 0000-0003-3314-9242

Present Address

#Department of Biochemistry, Faculty of Medicine, Khon Kaen University, Khon Kaen 40002, Thailand.

Notes

The authors declare no competing financial interest.

ACKNOWLEDGMENTS

We thank the Wellcome Trust (grant no. 097354/Z/11/Z), BBSRC (grant no. BB/M005666/1), and the University of Leeds for funding this project. Y.G. thanks the Wellcome Trust for supporting a career re-entry fellowship (grant no. 097354/Z/11/Z). E.P. thanks the University of Leeds and EPSRC for funding her a DTA Ph.D. studentship. C.S. thanks Khon Kaen University and its Faculty of Medicine for providing a Ph.D. studentship. We also thank Dr. M. Rowan Brown (Swansea University, UK) for the development of MATLAB scripts that enabled automation of nearest neighbour measurements in TEM images.

REFERENCES

(1) Bhatia, S.; Camacho, L. C.; Haag, R. *J. Am. Chem. Soc.* **2016**, *138*, 8654.
(2) Mammen, M.; Choi, S. K.; Whitesides, G. M. *Angew. Chem., Int. Ed.* **1998**, *37*, 2755.
(3) Bernardi, A.; Jimenez-Barbero, J.; Casnati, A.; De Castro, C.; Darbre, T.; Fieschi, F.; Finne, J.; Funken, H.; Jaeger, K. E.; Lahmann, M.; Lindhorst, T. K.; Marradi, M.; Messner, P.; Molinaro, A.; Murphy, P. V.; Nativi, C.; Oscarson, S.; Penades, S.; Peri, F.; Pieters, R. J.; Renaudet, O.; Reymond, J. L.; Richichi, B.; Rojo, J.; Sansone, F.; Schaffer, C.; Turnbull, W. B.; Velasco-Torrijos, T.; Vidal, S.; Vincent, S.; Wennekes, T.; Zuilhof, H.; Imberty, A. *Chem. Soc. Rev.* **2013**, *42*, 4709.
(4) Imperiali, B. *J. Am. Chem. Soc.* **2012**, *134*, 17835.
(5) Kiessling, L. L.; Grim, J. C. *Chem. Soc. Rev.* **2013**, *42*, 4476.
(6) Wu, F.; Jin, J.; Wang, L. Y.; Sun, P. F.; Yuan, H. X.; Yang, Z. Q.; Chen, G. S.; Fan, Q. H.; Liu, D. S. *ACS Appl. Mater. Interfaces* **2015**, *7*, 7351.
(7) Muller, C.; Despras, G.; Lindhorst, T. K. *Chem. Soc. Rev.* **2016**, *45*, 3275.
(8) Kitov, P. I.; Sadowska, J. M.; Mulvey, G.; Armstrong, G. D.; Ling, H.; Pannu, N. S.; Read, R. J.; Bundle, D. R. *Nature* **2000**, *403*, 669.
(9) Fan, E. K.; Zhang, Z. S.; Minke, W. E.; Hou, Z.; Verlinde, C.; Hol, W. G. J. *J. Am. Chem. Soc.* **2000**, *122*, 2663.
(10) Illescas, B. M. R. R.; Delgado, R.; Martín, N. *J. Am. Chem. Soc.* **2017**, *139*, 6018.
(11) Branson, T. R.; McAllister, T. E.; Garcia-Hartjes, J.; Fascione, M. A.; Ross, J. F.; Warriner, S. L.; Wennekes, T.; Zuilhof, H.; Turnbull, W. B. *Angew. Chem., Int. Ed.* **2014**, *53*, 8323.
(12) Marradi, M.; Chiodo, F.; Garcia, I.; Penades, S. *Chem. Soc. Rev.* **2013**, *42*, 4728.
(13) Ribeiro-Viana, R.; Sanchez-Navarro, M.; Luczkowiak, J.; Koeppe, J. R.; Delgado, R.; Rojo, J.; Davis, B. G. *Nat. Commun.* **2012**, *3*, 1303.
(14) Munoz, A.; Sigwalt, D.; Illescas, B. M.; Luczkowiak, J.; Rodriguez-Perez, L.; Nierengarten, I.; Holler, M.; Remy, J. S.; Buffet, K.; Vincent, S. P.; Rojo, J.; Delgado, R.; Nierengarten, J. F.; Martin, N. *Nat. Chem.* **2016**, *8*, 50.
(15) Geijtenbeek, T. B.; Kwon, D. S.; Torensma, R.; van Vliet, S. J.; van Duijnhoven, G. C.; Middel, J.; Cornelissen, I. L.; Nottet, H. S.; KewalRamani, V. N.; Littman, D. R.; Figdor, C. G.; van Kooyk, Y. *Cell* **2000**, *100*, 587.
(16) Geijtenbeek, T. B.; Torensma, R.; van Vliet, S. J.; van Duijnhoven, G. C.; Adema, G. J.; van Kooyk, Y.; Figdor, C. G. *Cell* **2000**, *100*, 575.
(17) Feinberg, H.; Mitchell, D. A.; Drickamer, K.; Weis, W. I. *Science* **2001**, *294*, 2163.
(18) Pohlmann, S.; Baribaud, F.; Lee, B.; Leslie, G. J.; Sanchez, M. D.; Hiebenthal-Millow, K.; Munch, J.; Kirchhoff, F.; Doms, R. W. *J. Virol.* **2001**, *75*, 4664.
(19) Kwon, D. S.; Gregorio, G.; Bitton, N.; Hendrickson, W. A.; Littman, D. R. *Immunity* **2002**, *16*, 135.
(20) Tabarani, G.; Thepaut, M.; Stroebel, D.; Ebel, C.; Vives, C.; Vachette, P.; Durand, D.; Fieschi, F. *J. Biol. Chem.* **2009**, *284*, 21229.
(21) Pohlmann, S.; Soilleux, E. J.; Baribaud, F.; Leslie, G. J.; Morris, L. S.; Trowsdale, J.; Lee, B.; Coleman, N.; Doms, R. W. *Proc. Natl. Acad. Sci. U. S. A.* **2001**, *98*, 2670.
(22) Wu, L.; KewalRamani, V. N. *Nat. Rev. Immunol.* **2006**, *6*, 859.
(23) Chung, N. P. Y.; Breun, S. K. J.; Bashirova, A.; Baumann, J. G.; Martin, T. D.; Karamchandani, J. M.; Rausch, J. W.; Le Grice, S. F. J.; Wu, L.; Carrington, M.; KewalRamani, V. N. *J. Biol. Chem.* **2010**, *285*, 2100.
(24) Guo, Y.; Feinberg, H.; Conroy, E.; Mitchell, D. A.; Alvarez, R.; Blixt, O.; Taylor, M. E.; Weis, W. I.; Drickamer, K. *Nat. Struct. Mol. Biol.* **2004**, *11*, 591.
(25) Feinberg, H.; Guo, Y.; Mitchell, D. A.; Drickamer, K.; Weis, W. I. *J. Biol. Chem.* **2005**, *280*, 1327.
(26) Davis, C. W.; Nguyen, H. Y.; Hanna, S. L.; Sanchez, M. D.; Doms, R. W.; Pierson, T. C. *J. Virol.* **2006**, *80*, 1290.
(27) Menon, S.; Rosenberg, K.; Graham, S. A.; Ward, E. M.; Taylor, M. E.; Drickamer, K.; Leckband, D. E. *Proc. Natl. Acad. Sci. U. S. A.* **2009**, *106*, 11524.
(28) Diehl, C.; Engstrom, O.; Delaine, T.; Hakansson, M.; Genheden, S.; Modig, K.; Leffler, H.; Ryde, U.; Nilsson, U. J.; Akke, M. *J. Am. Chem. Soc.* **2010**, *132*, 14577.
(29) Holla, A.; Skerra, A. *Protein Eng., Des. Sel.* **2011**, *24*, 659.
(30) Linman, M. J.; Taylor, J. D.; Yu, H.; Chen, X.; Cheng, Q. *Anal. Chem.* **2008**, *80*, 4007.
(31) Bruchez, M.; Moronne, M.; Gin, P.; Weiss, S.; Alivisatos, A. P. *Science* **1998**, *281*, 2013.
(32) Chan, W. C. W.; Nie, S. M. *Science* **1998**, *281*, 2016.
(33) Michalet, X.; Pinaud, F. F.; Bentolila, L. A.; Tsay, J. M.; Doose, S.; Li, J. J.; Sundaresan, G.; Wu, A. M.; Gambhir, S. S.; Weiss, S. *Science* **2005**, *307*, 538.
(34) Medintz, I. L.; Clapp, A. R.; Mattoussi, H.; Goldman, E. R.; Fisher, B.; Mauro, J. M. *Nat. Mater.* **2003**, *2*, 630.
(35) Zhou, D. *Biochem. Soc. Trans.* **2012**, *40*, 635.
(36) Wegner, K. D.; Hildebrandt, N. *Chem. Soc. Rev.* **2015**, *44*, 4792.
(37) Hildebrandt, N.; Spillmann, C. M.; Algar, W. R.; Pons, T.; Stewart, M. H.; Oh, E.; Susumu, K.; Diaz, S. A.; Delehanty, J. B.; Medintz, I. L. *Chem. Rev.* **2017**, *117*, 536.
(38) Chinen, A. B.; Guan, C. M.; Ferrer, J. R.; Barnaby, S. N.; Merkel, T. J.; Mirkin, C. A. *Chem. Rev.* **2015**, *115*, 10530.
(39) Zhang, C. Y.; Yeh, H. C.; Kuroki, M. T.; Wang, T. H. *Nat. Mater.* **2005**, *4*, 826.

DOI: 10.1021/jacs.7b05104
J. Am. Chem. Soc. 2017, 139, 11833−11844

(40) Zhou, D. J.; Bruckbauer, A.; Abell, C.; Klenerman, D.; Kang, D. J. *Adv. Mater.* **2005**, *17*, 1243.
(41) Somers, R. C.; Bawendi, M. G.; Nocera, D. G. *Chem. Soc. Rev.* **2007**, *36*, 579.
(42) Howarth, M.; Liu, W.; Puthenveetil, S.; Zheng, Y.; Marshall, L. F.; Schmidt, M. M.; Wittrup, K. D.; Bawendi, M. G.; Ting, A. Y. *Nat. Methods* **2008**, *5*, 397.
(43) Zhang, H.; Zhou, D. *Chem. Commun.* **2012**, *48*, 5097.
(44) Benito-Alifonso, D.; Tremel, S.; Hou, B.; Lockyear, H.; Mantell, J.; Fermin, D. J.; Verkade, P.; Berry, M.; Galan, M. C. *Angew. Chem., Int. Ed.* **2014**, *53*, 810.
(45) Lee, J.; Brennan, M. B.; Wilton, R.; Rowland, C. E.; Rozhkova, E. A.; Forrester, S.; Hannah, D. C.; Carlson, J.; Shevchenko, E. V.; Schabacker, D. S.; Schaller, R. D. *Nano Lett.* **2015**, *15*, 7161.
(46) Wang, Q.; Liu, Y.; Ke, Y.; Yan, H. *Angew. Chem., Int. Ed.* **2008**, *47*, 316.
(47) Guo, Y.; Sakonsinsiri, C.; Nehlmeier, I.; Fascione, M. A.; Zhang, H.; Wang, W.; Poehlmann, S.; Turnbull, W. B.; Zhou, D. *Angew. Chem., Int. Ed.* **2016**, *55*, 4738.
(48) Susumu, K.; Uyeda, H. T.; Medintz, I. L.; Pons, T.; Delehanty, J. B.; Mattoussi, H. *J. Am. Chem. Soc.* **2007**, *129*, 13987.
(49) Aldeek, F.; Hawkins, D.; Palomo, V.; Safi, M.; Palui, G.; Dawson, P. E.; Alabugin, I.; Mattoussi, H. *J. Am. Chem. Soc.* **2015**, *137*, 2704.
(50) Mei, B. C.; Susumu, K.; Medintz, I. L.; Mattoussi, H. *Nat. Protoc.* **2009**, *4*, 412.
(51) Song, L.; Ho, V. H. B.; Chen, C.; Yang, Z. Q.; Liu, D. S.; Chen, R. J.; Zhou, D. J. *Adv. Healthcare Mater.* **2013**, *2*, 275.
(52) Ma, L.; Tu, C. L.; Le, P.; Chitoor, S.; Lim, S. J.; Zahid, M. U.; Teng, K. W.; Ge, P. H.; Selvin, P. R.; Smith, A. M. *J. Am. Chem. Soc.* **2016**, *138*, 3382.
(53) Liu, D.; Snee, P. T. *ACS Nano* **2011**, *5*, 546.
(54) Liu, W. H.; Greytak, A. B.; Lee, J.; Wong, C. R.; Park, J.; Marshall, L. F.; Jiang, W.; Curtin, P. N.; Ting, A. Y.; Nocera, D. G.; Fukumura, D.; Jain, R. K.; Bawendi, M. G. *J. Am. Chem. Soc.* **2010**, *132*, 472.
(55) Muro, E.; Pons, T.; Lequeux, N.; Fragola, A.; Sanson, N.; Lenkei, Z.; Dubertret, B. *J. Am. Chem. Soc.* **2010**, *132*, 4556.
(56) Kong, L.; Wilson, I. A.; Kwong, P. D. *Proteins: Struct., Funct., Genet.* **2015**, *83*, 590.
(57) Stewart-Jones, G. B. E.; Soto, C.; Lemmin, T.; Chuang, G. Y.; Druz, A.; Kong, R.; Thomas, P. V.; Wagh, K.; Zhou, T. Q.; Behrens, A. J.; Bylund, T.; Choi, C. W.; Davison, J. R.; Georgiev, I. S.; Joyce, M. G.; Do Kwon, Y.; Pancera, M.; Taft, J.; Yang, Y. P.; Zhang, B. S.; Shivatare, S. S.; Shivatare, V. S.; Lee, C. C. D.; Wu, C. Y.; Bewley, C. A.; Burton, D. R.; Koff, W. C.; Connors, M.; Crispin, M.; Baxa, U.; Korber, B. T.; Wong, C. H.; Mascola, J. R.; Kwong, P. D. *Cell* **2016**, *165*, 813.
(58) Zhang, H.; Li, S.; Lu, R.; Yu, A. *ACS Appl. Mater. Interfaces* **2015**, *7*, 21868.
(59) Zhang, H.; Feng, G.; Guo, Y.; Zhou, D. *Nanoscale* **2013**, *5*, 10307.
(60) Lee, J. H.; Ozorowski, G.; Ward, A. B. *Science* **2016**, *351*, 1043.
(61) Hondow, N.; Brydson, R.; Wang, P.; Holton, M. D.; Brown, M. R.; Rees, P.; Summers, H. D.; Brown, A. *J. Nanopart. Res.* **2012**, *14*, 1 DOI: 10.1007/s11051-012-0977-3.
(62) Mitchell, G. P.; Mirkin, C. A.; Letsinger, R. L. *J. Am. Chem. Soc.* **1999**, *121*, 8122.
(63) Samanta, A.; Zhou, Y.; Zou, S.; Yan, H.; Liu, Y. *Nano Lett.* **2014**, *14*, 5052.
(64) Kong, Y. F.; Chen, J.; Fang, H. W.; Heath, G.; Wo, Y.; Wang, W. L.; Li, Y. X.; Guo, Y.; Evans, S. D.; Chen, S. Y.; Zhou, D. J. *Chem. Mater.* **2016**, *28*, 3041.

DOI: 10.1021/jacs.7b05104
J. Am. Chem. Soc. 2017, 139, 11833−11844